Synthesis of MnCo$_2$O$_4$ nanoparticles as modifiers for simultaneous determination of Pb(II) and Cd(II)

Vesna Antunović[1]ᵒ, Marija Ilić[2]ᵒ, Rada Baošić[3]ᵒ, Dijana Jelić[1]ᵒ, Aleksandar Lolić[3]ᵒ *

1 Faculty of Medicine, University of Banja Luka, Banja Luka, Bosnia and Herzegovina, **2** University of Belgrade—Faculty of Mining and Geology, Belgrade, Serbia, **3** Department of Analytical Chemistry, University of Belgrade—Faculty of Chemistry, Belgrade, Serbia

ᵒ These authors contributed equally to this work.
* lolix@chem.bg.ac.rs

Data Availability Statement: All relevant data are within the manuscript and its Supporting Information files.

Competing interests: The authors have declared that no competing interests exist.

Abstract

The porous spinel oxide nanoparticles, MnCo$_2$O$_4$, were synthesized by citrate gel combustion technique. Morphology, crystallinity and Co/Mn content of modified electrode was characterized and determined by Fourier transform infra-red spectroscopy (FT-IR), scanning electron microscopy (SEM), energy dispersive spectrometry (EDS), X-ray diffraction pattern analysis (XRD), simultaneous thermogravimetry and differential thermal analysis (TG/DTA). Nanoparticles were used for modification of glassy carbon electrode (GCE) and new sensor was applied for simultaneous determination of Pb(II) and Cd(II) ions in water samples with the linear sweep anodic stripping voltammetry (LSASV).The factors such as pH, deposition potential and deposition time are optimized. Under optimal conditions the wide linear concentration range from 0.05 to 40 μmol/dm^3 was obtained for Pb(II), with limit of detection (LOD) of 8.06 nmol/dm^3 and two linear concentration ranges were obtained for Cd(II), from 0.05 to 1.6 μmol/dm^3 and from 1.6 to 40 μmol/dm^3, with calculated LOD of 7.02 nmol/dm^3. The selectivity of the new sensor was investigated in the presence of interfering ions. The sensor is stable and it gave reproducible results. The new sensor was succesfully applied on determination of heavy metals in natural waters.

Introduction

Spinel structures with general formula AB$_2$O$_4$ are well known materials in the field of catalysis, especially in the area of neutralizing the harmful components from environment, such as heavy metals [1,2]. Contamination of heavy metal ions is one of the most serious environmental issues, since heavy metal ions are not biodegradable and they accumulate in living organisms, tracking the heavy metal concentration in environment is of utmost importance. Heavy metal content is often quantified by well-known analytical methods, such as atomic absorption spectrometry (AAS) [3,4] inductively coupled plasma-mass spectrometry (ICP-MS) [5,6], inductively coupled plasma-optical emission spectrometry (ICP-OES) [7,8]and X-ray fluorescence spectrometry (XRF) [9]. Besides numbered techniques, electrochemical methods are also often used in analysis of heavy metals, mostly due to their high sensitivity, easy operation

and transferability [10–12]. Modification of electrode surface by nanostructures such as carbon nanotubes (CNT), graphene or nanoparticles is one of the strategies for surface modification. Numerous papers reported electrode modification such as Cu-CeO$_2$ coated with multiwall carbon nanotubes for determination of guanine and adenine [13] or Fe$_3$O$_4$/RGO nanoparticles for glassy carbon electrode modification for detection of Cd(II) ions [14]. Determination of various ions such as Zn(II), Cd(II), Pb(II), Cu(II) and Ag(I) using electrode modified with chromium oxide were reported [11].ZnO are often used as sensing devices in chemical, pharmaceutical and/or agricultural applications [15,16], the group of authors investigated the application of graphene nanoparticles on environmental pollutants and detection of Al(III) ions [17,18].

Present paper focus on spinel structure material that consist of Mn(II) and Co(II) combined in formula MnCo$_2$O$_4$, where Mn(II) occupies tetrahedral and Co(II) octahedral sites of crystal structure and its application for catching Cd(II) and Pb(II) ions in water samples. Spinel structure containing 3d elements, such as Mn and Co, or Fe, Cr and Ni have high spin electron configuration, due to oxygen ions being a weak field ligand. A great potential of MnCo$_2$O$_4$ in electrocatalysis [19] and in efficiency in polymer degradation [20] was reported. In order to make a good material with all good and desirable physicochemical characteristics, method of synthesis is very important. There are numerous papers concerning methods of synthesis of different spinel nanostructures, for electrochemical purpose, such as co-precipitation [21,22], sol–gel method [23,24], microemulsion method [25], hydrothermal [26], spray pyrolysis [27]. For Mn-Co spinel structure the most implemented methods are precipitation [1,28,29], hydrothermal method [30,31], combustion synthesis [32], or impregnation reaction [33]. It should be mentioned here that choice of precursor is also very important, since using hydroxides in precipitation reaction produce small surface area and possibility of shrinking the active surface very quickly [34]. The use of individual transition metals proved to be very good choice for synthesis of materials with specific surface area up to 100 m^2/g which are thermally stable up to 500˚C. Several precursors containing Mn and Co ions were used for spinel structure preparation such as: citrates [35], acetates [36], hydroxycarbonates [37], carbonates [35] and chlorides [1,29]. In this paper MnCo$_2$O$_4$ was synthesized by citrate-gel combustion technique. This sol-gel auto combustion technique is quite common, provides a very good homogeneity of samples, very easy control of stoichiometry and production at low cost. The proposed method involves metal salt (oxidizer) and organic complexant (reductant). Different salts can be used as precursors for auto-combustion technique but nitrates are the most commonly used. Furthermore, nitrates are hygroscopic and they absorb moisture well [38,39]. Citrate acid was used here as a fuel (reductant) in synthesis. Other chemicals, such as urea or glycin can also be used as a reductant. Glycine as as fuel was used for combustion synthesis of mesoporous MnO$_2$/MnCo$_2$O$_4$ composite [32]. The choice of fuel, as well as the ratio of oxidizer/fuel affects morphology and electrochemical properties of electrode material [32,38].

Auto-combustion method is well known for production of nanodispersed simple or complex oxide, catalyst, superconductors etc. This synthesis method is quite common for synthesis of spinel-type ferrite nanomaterials [38], but according to authors' knowledge, there are no previously published papers describing the synthesis of MnCo$_2$O$_4$ nanoparticles by citrate-gel combustion technique for simultaneous determination of Cd(II) and Pb(II).

Materials and methods

Chemicals

Manganese nitrate, cobalt nitrate, 25% ammonium hydroxide and citric acid were obtained from Carlo Erba (Val de Ruil, France). Sulfuric acid (98%), acetic acid (98%), sodium acetate

and potassium chloride were obtained from Betahem (Belgrade, Serbia). Working Pb(II) and Cd(II) were prepared from stock solutions used for atomic absorption (1000 ppm each, Merck). All reagents were analytical grade quality and used without further purification. Ultrapure water (Mili-Q plus 185, system Milipore) was used for preparation of all solutions.

Preparation of supporting electrolytes

The solutions used as supporting electrolytes were prepared as follows: The H_2SO_4/KCl buffer solution was prepared by mixing equal volumes of the 20 mmol/dm^3 sulfuric acid and 30 mmol/dm^3 potassium chloride for pH 2. The acetate buffer solutions with different value from pH 4–6, were prepared by mixing appropriate volumes of 0.1 mol/dm^3 acetic acid and 0.1 mol/dm^3 sodium-acetate solutions.

Instrumentation

Fourier transform infra-red spectroscopy (FT-IR) was carried out by using Tensor 27 instrument with addition of platinum stand on which a very small amount of spinel oxides sample was placed (Bruker, USA). The particle size and morphology of $MnCo_2O_4$ powder was observed by scanninig electron microscope (SEM) JEOL JSM-6390 LV. The X-ray diffractograms of the $MnCo_2O_4$ samples were obtained by means of Philips PW-1050 automatic diffractometer with a Cu K□1,2 line of 0.15418 nm. All electrochemical measurements were performed using a CHI 800C workstation (CH Instruments, USA). A three electrode system consisted of the glassy carbon working electrode (GCE; bare or modified), (CH instruments, USA; model CHI104), 3 mm in diameter. As reference electrode was used Ag/AgCl (CH Instruments, USA; CHI111) and platinum wire as auxiliary electrode.

Synthesis of $MnCo_2O_4$ spinel oxide nanoparticles

Synthesis of $MnCo_2O_4$ spinel oxide nanoparticles was carried out by citrate-gel combustion method. Manganese nitrate and cobalt nitrate solutions were mixed in molar ratio 1:2. Citric acid was used as a fuel. The mole ratio of citric acid versus nitrate groups was 1:3.6 as published elsewhere [40]. The pH 7 is adjusted by adding a solution of ammonium hydroxide. Solution was heated in an open glass beaker at temperature around 80˚C under constant stirring (100 rpm) until light pink sol was formed. The sol turn into gel and it was finally calcinated for 2h at 450˚C. The combustion of citric acid is presented by following equation (Eq 1):

$$2C_6H_8O_7 + 9O_2 \rightarrow 12CO_2 + 8H_2O \tag{1}$$

Since the combustion temperature needed to complete combustion of remaining carbon residues is unknown, the heating at a constant temperature of 500˚C was prolonged for approximately half an hour, which was enough to obtain carbon-free oxides. After calcination, a black powder of $MnCo_2O_4$ nanoparticles (NPs) was obtained.

Preparation of glassy carbon electrode modified with $MnCo_2O_4$ nanoparticles

Before modification, working electrode was pre-cleaned on a polishing pad using alumina slurry with different grain sizes (1, 0.3, and 0.05 μm, Buehler, USA). The electrode was rinsed with Mili Q water and methanol and ultrasonically dispersed for 3 min in a mixture of methanol and water (1:1, v/v). Suspension for modification was made by adding 1 mg of $MnCo_2O_4$ powder in 2 cm^3 of pure water followed by sonication for 30 min. A 6 μL of the $MnCo_2O_4$

suspension was injected onto glassy carbon (GCE) mirror clean surface allowing the water evaporate at room temperature. The modified electrode is denoted as GCE-MnCo$_2$O$_4$NPs.

Analytical procedure

The electrochemical measurements were performed in a three-electrode cell with a glassy carbon (bare or modified) electrode as the working electrode, a Ag/AgCl as the reference electrode, and a platinum wire as an auxiliary electrode. For pre-concentration step, the GCE-MnCo$_2$O$_4$NPs modified electrode was immersed into a H$_2$SO$_4$/KCl supporting electrolyte containing Pb(II) and Cd(II), and the accumulation and reduction of metal ions into metal (M^{2+} to M^0) was performed under a constant potential at -1.4 V for 10 minutes with stirring. The deposition process was followed by the opposite process: re-oxidation of metals (M^0) and stripping into solution metal ions (M^{2+}). The electrochemical response was measured by linear sweep anodic stripping voltammetry (LSASV) in the potential range from -1.0 to 0 V vs. Ag/AgCl electrode with the scan in the anodic direction (re-oxidation of metal M^0 to M^{2+}). All electrochemical measurements are performed in triplicate (unless otherwise stated) and numbers are average values with apropriate confidence interval.

Preparation of water samples

The application of the proposed sensor was performed by measuring the content of Pb(II) and Cd(II) in water samples. We used three different water samples: distilled water, tap water, and river water. River water samples were collected from Danube river (44°49′49″N and 20°27′47.5″E) on its right bank, closer to the Belgrade city centre, and tap water samples were collected from inside the faculty building (University of Belgrade, Faculty of Chemistry). Distilled and tap water samples were used without any prior preparation, while the sample of river water was filtered (membrane filter pore size 0.45 μm). Samples were prepared as follows: the appropriate volumes of the standard Pb(II) and Cd(II) solutions were transferred to a volumetric flask containing 2 cm^3 of a water sample and 8 cm^3 of supporting electrolyte. To remove dissolved oxygen through the prepared solutions, pure nitrogen was passed. Every sample was prepared in triplicate.

Results and discussion

Characterization of the MnCo$_2$O$_4$spinel material

FT-IR spectrum was observed in the range of 4000–400 cm^{-1} (Fig 1) which is usual for ion vibrations in the crystal lattice. The most prominent absorption bands at 610 cm^{-1} and 460 cm^{-1} are corresponding to metal-oxygen bonds in spinel structure of composite. Similar reports were for absorption peaks appearing in the range of 569–616 cm^{-1} represent high frequency bands which are characteristic of metal-oxygen vibrations in tetrahedral sites, while absorption peaks in the range of 426–471 cm^{-1} represent low frequency bands and this is caused by vibration of octahedral sites metal-oxygen bond [41]. Due to high temperature during the combustion process hydroxyl and nitrate groups are eliminated fromspinel material. The FTIR image also shows absorption band at ~2400 cm^{-1} which probably originates from adsorbed water molecules on the surface of MnCo$_2$O$_4$ nanoparticles [42,43].

Presence of water was also detected by simultaneous TG/DTA analysis around 100°C presented with diffuse endothermic peak. Thermal analysis showed a very good thermal stability of prepared material in the temperature range from ambient up to 950°C, since mass loss presented in TG curve is quite insignificant and gradual disintegration of MnCo$_2$O$_4$ was not observed (Fig 2).
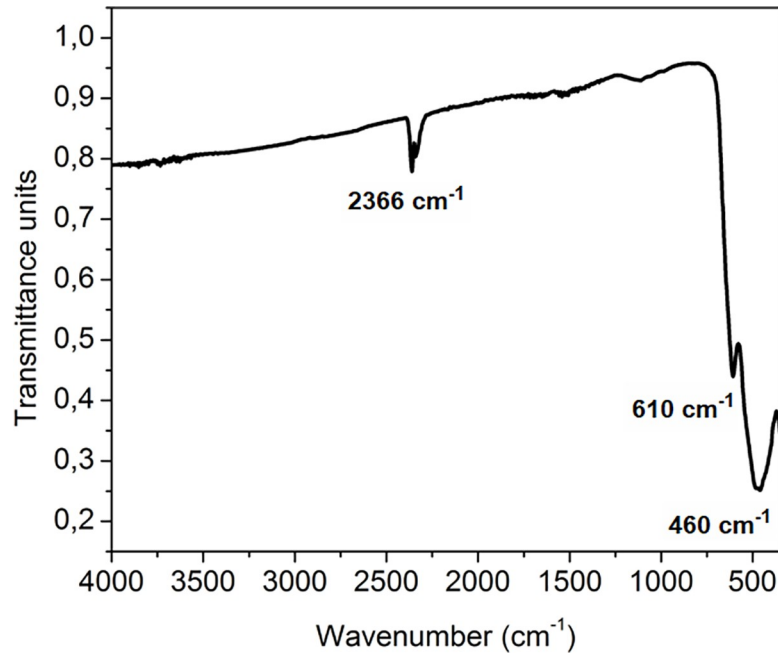
Fig 1. FTIR spectrum of MnCO$_2$O$_4$ nanoparticles in the spectrum range from 400 to 4000 cm^{-1}.

https://doi.org/10.1371/journal.pone.0210904.g001

A representative X-ray diffraction patterns of the as-prepared final product is shown in Fig 3. Obtained X-ray spectrum shows to be in consistent with standard pattern of spinel structure of cubic MnCo$_2$O$_4$ with theoretical density of 5.564 g/cm (JCPDS card No. 23–1237) regarding on some diffraction peak positions. The results were consistent with results previously reported [42,44,45]. Diffraction peaks are corresponding to the Miller indices (111), (220), (311), (400), (422), (511), (440) and (533) revealed face-centered cubic spinel structure of the MnCo$_2$O$_4$[43,45]The most intense lines at 2θ of 18.53, 30.47, 35.99, 43.64, 54.30, 57.84, 63.45 degrees in XRD pattern are in good agreement with the angles (18.55, 30.54, 35.995, 43.759,
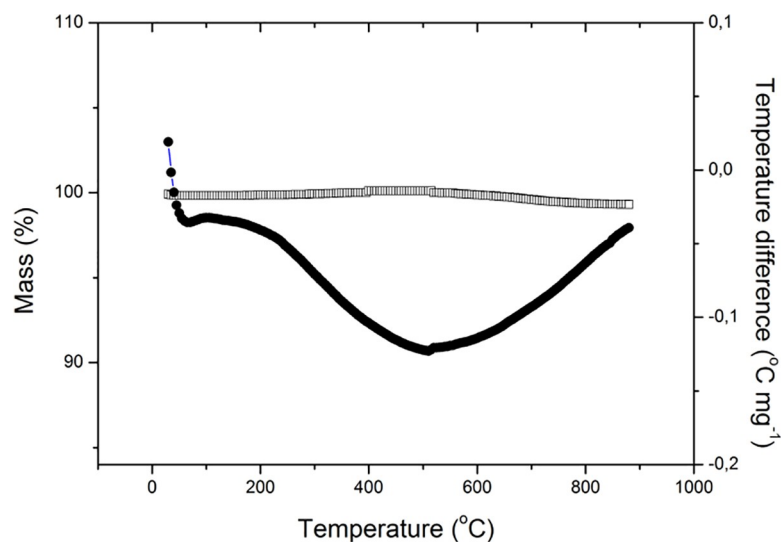

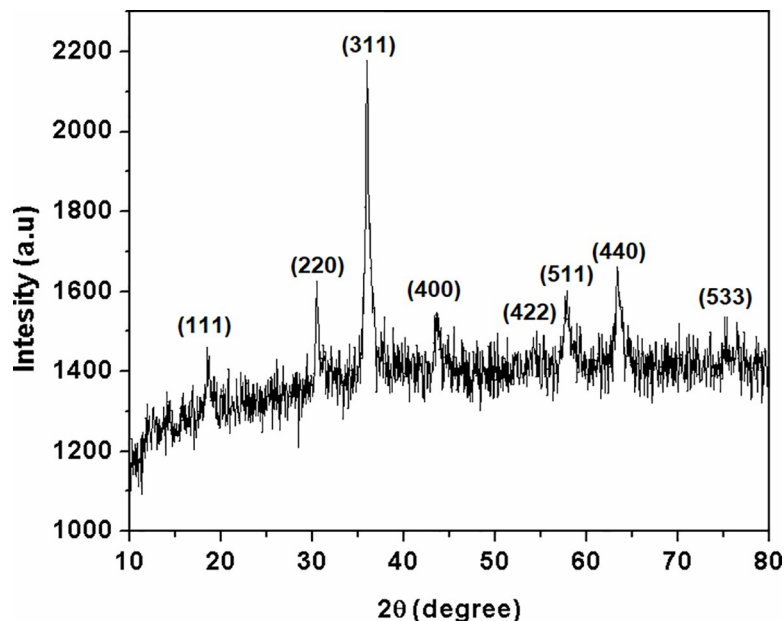**Fig 2. TG/DTA analysis of MnCo$_2$O$_4$ nanoparticles.**

https://doi.org/10.1371/journal.pone.0210904.g002

Fig 3. XRD pattern of 0.5MnO-0.5Co$_2$O$_4$ oxide system synthesized by citrate-gel combustion technique. The diagram indicates poorly crystallized (semiamorphous) MnCo$_2$O$_4$.

54.336, 57.909, and 63.622) in JCPDS card of MnCo$_2$O$_4$. As-prepared MnCo$_2$O$_4$ shows some nosier XRD spectrum than standard pattern of spinel structure of MnCo$_2$O$_4$ which is probably caused by low crystallite size [1,42]. In this case, Debye-Scherrer formula (Eq 2) based on full width at half maximum intensity of the (311) peak of the as-prepared MnCo$_2$O$_4$ can be used to calculate the average crystallite size which was amount to 19 nm.

$$D = 0.9\alpha/(\beta\cos\theta). \qquad (2)$$

SEM images (Fig 4) show porous morphology of MnCo$_2$O$_4$. Flower-like structure is pronounced on the micrographs. Different polygonal particles are spread over the flower surface. Some cracks and defects are also visible. Morphological structure contains pores which probably allow transport of electrolyte, providing a good surface area for charge transfer reactions. This kind of ultrathin flow-like morphologies posses high electrochemical capacity which is responsible for efficient transport of electrons and ions [42,46]. As mentioned before this way of synthesis provides a good homogeneity of the nanocomposite which is mostly achieved with 1 to 1 molar ratio of the components [40]Assuming an almost spherical shape and accepting the mean particle radius r = 19 nm, the specific surface area was estimated on the basis of equation [47,48]

$$S = 3/rd. \qquad (3)$$

Where d is the bulk density 5.564 g/cm was used. This calculation gave us the value of 28.37 m^2/g.

Elemental composition analysis (Fig 5) of this porous spinel material obtained from energy dispersive spectrometer (EDS) further confirms the existence of manganese, cobalt and oxygen with weight percentage of 6.06%, 7.54% and 86.39%.
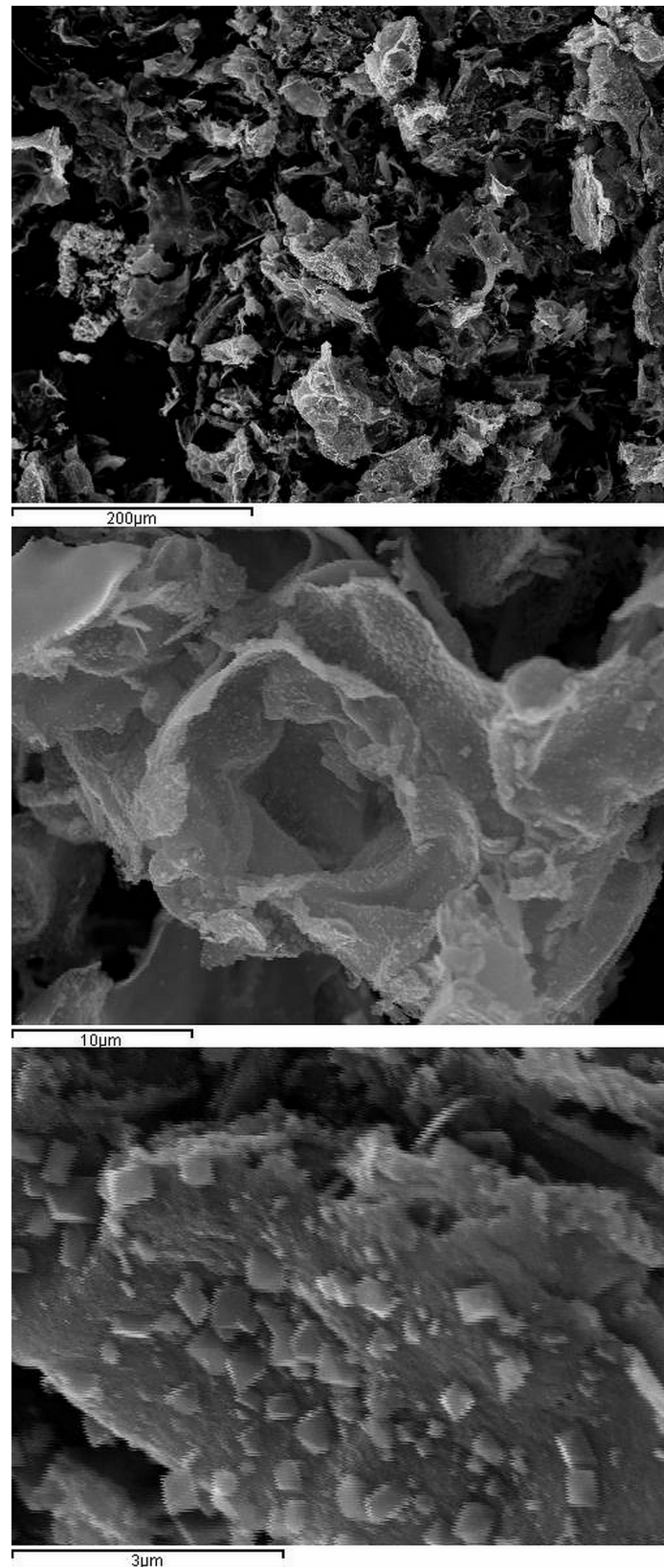
Fig 4. The SEM microphotographs of MnCo$_2$O$_4$ samples obtained with the temperature Tf = 500˚C.
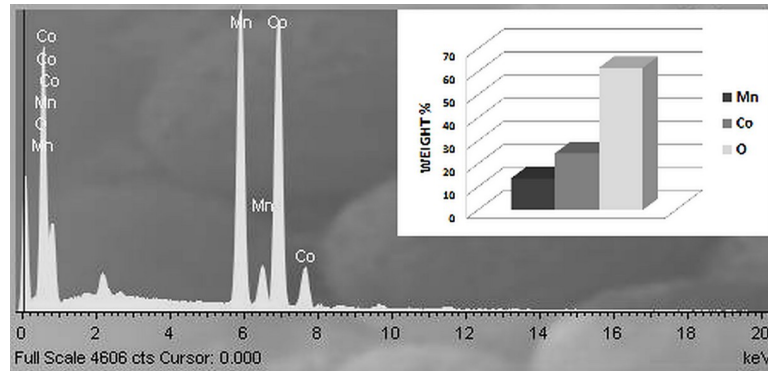
Fig 5. EDS spectrum for 0.5MnO-0.5Co$_2$O$_4$ and element weight bar (%) diagram (13.7%, 24.58% and 61.72% for manganese, cobalt and oxygen, respectively).

Electrochemical performance of the GCE-MnCo$_2$O$_4$NPs

Cyclic voltammograms of the sensor were recorded in the presence of 10 μmol/dm^{3}Cd(II) and Pb(II) ions at a scan rate of 150 mV/s in H$_2$SO$_4$/KCl buffer (pH 2). Fig 6 shows voltammograms obtained for both bare and modified glassy carbon electrode. As it can be seen from the figure there are no visible signals on bare electrode whereas on the modified there are two well defined peaks at -500mV and -750 mV. The first peak was assigned to reduction of lead and second to cadmium, this finding was confirmed by recording cyclic voltammograms of solutions of individual ions (not shown here).

Electrochemical performance of the sensor was investigated by linear sweep voltammetry (LSV). LSVs on both bare and GCE-MnCo$_2$O$_4$NPs show increased sensitivities for both analytes on modified electrode. Obtained peak currents for Pb(II) and Cd(II) on modified electrode were 24.7 and 25.4 μA, they are two times more sensitive for Pb(II) and six times more
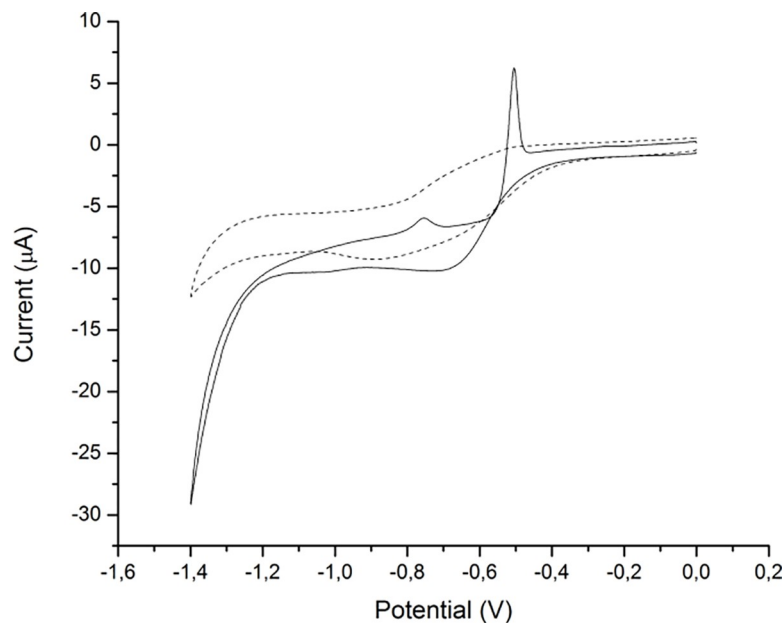

Fig 6. Cyclic voltammograms obtained on bare (dashed) and modified glassy carbon electrode (solid) for 10 μmol/dm^{3}Pb(II) and Cd(II) at 150 mV/s scan rate.
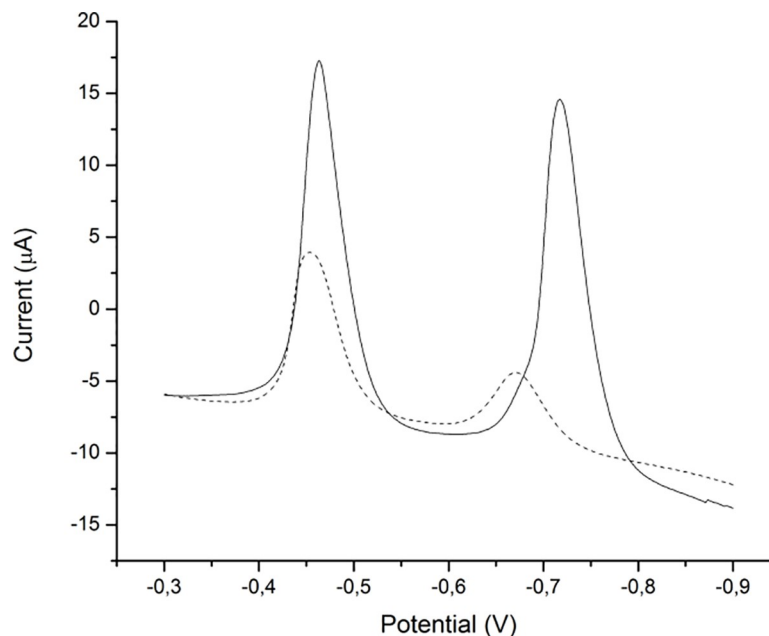
Fig 7. Comparison of LSAS voltammograms obtained for 1 μmol/dm³ Pb(II) and Cd(II) on bare (dashed) and on modified GCE (solid).

https://doi.org/10.1371/journal.pone.0210904.g007

sensitive for Cd(II), obtained peak currents for bare electrode were 11.2 and 4.1 μA (Fig 7). The large difference in stripping potentials (250 mv) between the well defined peaks of Cd(II) and Pb(II) made simultaneous detection of these two ions in aqueous media by LSASV technique possible. Since the modified electrode has increased surface area due to the presence of the nanoparticles it has improved sensitivity toward the analytes. The larger surface area increase the number of active sites and it leads to higher signal-to-noise ratio [49].In order to achieve the best experimental conditions for determination of lead and cadmium content, the influence of pH, accumulation time and accumulation potential were examined.

Effect of pH

The effect of the pH value of the supporting electrolyte on the voltammetric response of Pb(II) and Cd(II) was examined in the pH range 2–6. In order to achieve the value pH 2 of the supporting electrolyte, a mixture of 20 mmol/dm³ sulfuric acid and 30 mmol/dm³ potassium chloride was used, as reported elsewhere [33] and for pH 4 to 6 range, the 0.1 mol/dm³ acetate buffer was used [50–52]. It is worth to mention that there are some discrepancies in literature concerning this issue. $NiCo_2O_4$ spinel structure showed lack of stability and electrochemical activity in acidic media [53] while synthesized cobalt ferrit spinel structure by hydrothermal technique confirmed stability of $CoFe_2O_4$ nanoparticles in a wide range of pH 2.2 to 10.8 [54]. From our experimental results a large, well defined and sharp current peaks, for both Pb(II) and Cd(II), appear in H_2SO_4/KCl buffer (pH 2), while acetate buffer (pH 4–6) gave less defined and intensive current peaks presented in Fig 8. The smallest concentration of Cd(II) that gives current peak in acetate buffer is 0.2 μmol/dm³ while in the H_2SO_4/KCl it is four times smaller.

The Fig 9 shows barely visible peak of the of 0.2 μmol/dm³ Cd(II) in acetate buffer (pH 4) while the same concentration in the H_2SO_4/KCl buffer gives a clear and much larger peak. This occurrence could be attributed to complex formation between metal ions and acetate
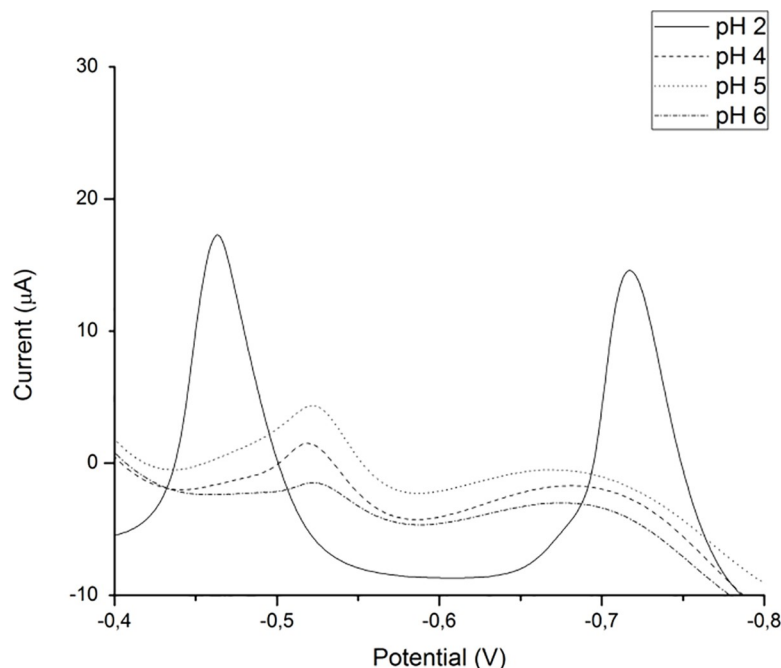
Fig 8. Effect of pH on Pb(II) and Cd(II) LSAS signals (concentration 1 μmol/dm^3 for both Pb(II) and Cd(II)).

buffer [55]. Electrochemical behavior of citrate-gel synthesized $MnCo_2O_4$ spinel material in H_2SO_4/KCl buffer is in a good agreement with observation for MnO_2/carbon composites [33].

Effect of accumulation time and potential

The dependence of the linear sweep anodic stripping current peaks of Pb(II) and Cd(II) on the accumulation time and accumulation potential were examined. During deposition all solutions were stirred on a magnetic stirrer. As can be seen in Fig 10 accumulation potential and accumulation time have great influence on current intensities so they represent important steps in the optimization process. The effect of accumulation potential was investigated in the range from -1.0 to -1.5V, while the accumulation time was kept constant at 600 seconds. The highest peak was at potential -1.4 V and Fig 10A shows that even small potential change causes a significant increase of the oxidation current for both Pb(II) and Cd(II). Such behavior could be attributed to hydrogen adsorption onto surface of working electrode which was observed before [10,56]. Examination of accumulation time was investigated in the range 50–650 seconds at constant potential -1.4 V. As can be seen from the Fig 10B the current peaks for both Pb(II) and Cd(II) increase to 600 s and then become constant as is described previously [57]. Hence the optimal deposition conditions for simultaneous determination of Pb(II) and Cd(II) on GCE- $MnCo_2O_4$NPs were: accumulation potential of –1.4 V vs. Ag/AgCl, accumulation time of 600 s at pH 2 (H_2SO_4/HCl buffer).

Interference study

In order to evaluate the selectivity of the proposed sensor GCE-$MnCo_2O_4$NPs, we examined the influence of some inorganic ions on the voltammetric response of Pb(II) and Cd(II). The experiment was performed by mixing solutions of common inorganic ions such as Mn(II), Zn(II), Cr(II), Hg(II), Cu(II) and Ni(II) with a solution containing 1.0 μmol/dm^3 of Pb(II) and

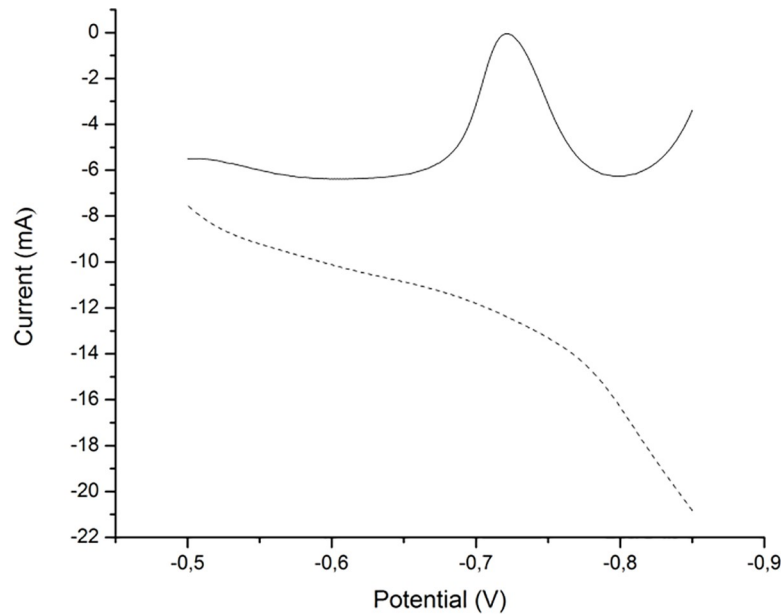**Fig 9. LSAS voltammogram obtained for 0.2 μmol/dm^{3}Cd(II) in acetate buffer (pH 4) (dashed) and in H$_2$SO$_4$/KCl buffer, pH 2 (solid).**

Cd(II). The ions present in water in abundant concentrations were also investigated K(I), Mg (II), and Ca(II). The concentration of potentially interfering ions was up to ten times higher than the concentration of Pb(II) and Cd(II) in solution. The obtained results are displayed in Table 1. As can be seen, the significant interference was only pronounced for copper ions. This interference can be related to migration and diffusion processes developing separately. It was reported previously that if sulfuric acid is used as a supporting electrolyte where copper sulfate is present as it is in our case, it can enhance conductivity and transference number of cupric ion [58]. Sulfuric acid also increases the diffusion and reduces the migration of copper ions, and this can be one of the reasons for significant interference of copper ions [58]. As previously suggested, this interference can be effectively overcome by the addition of Ferro-cyanide ions which creates a stable complex with Cu(II) and mask the copper ions [59].

Calibration data and application parameters

Under optimised parameters the linearity of the new sensor was investigated by recording of standard solutions of both analytes in the concentration range 0.05–40 μmol/dm^3. The
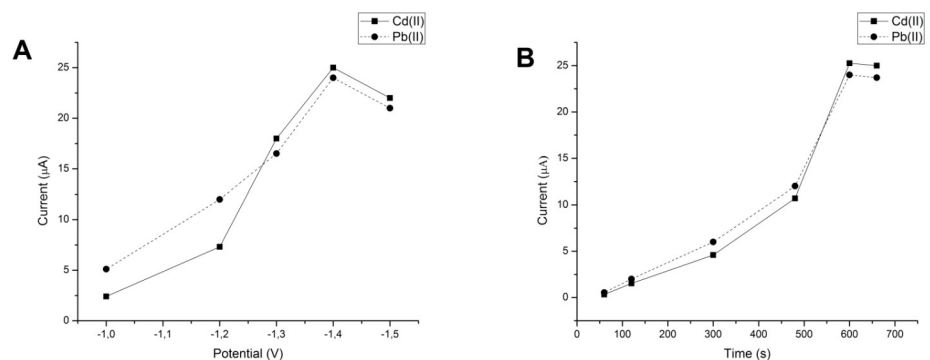

Fig 10. Dependance of oxidation current on accumulation potential (A) and time (B) of 1 μmol/dm^3 Pb(II) and Cd (II).

Table 1. Interference study of some metal ions (10 μmol/dm³) on the voltammogram responses of 1 μmol/dm³Pb (II) and Cd(II). Supporting electrolyte: H₂SO₄/KCl (pH 2); deposition potential: -1.4 V, deposition time: 10 min; working electrode GCE-MnCo₂O₄NPs.

Intereferant	Peak current change (%)	
	Pb(II)	**Cd(II)**
K(I)	-3	-3
Mg(II)	+3	+2
Ca(II)	-1	-3
Mn(II)	-2	+1
Zn(II)	+6	+8
Cu(II)	-40	-36
Hg(II)	-7	-8
Cr(III)	-3	+1
Ni(II)	-3	-1

calibration curve and LSAS voltammograms for different concentration of Pb(II) and Cd(II) are presented in Fig 11. As seen from the Figure there is shift in peak potential with concentration of analytes. This phenomenon is observed in papers describing modification of GCE with various nanoparticles. In Fig 11, it can be seen that there is a slight displacement of the peak potentials, in case of Cd(II) only. This displacement can be attributed to overlapping of diffusion layers resulting from the stripping of metal (M^0) from the surface of the electrode and the transition of metal ions (M^{2+}) into the solution [57]. Linear ranges of the proposed method were from 0.05 to 40 μmol/dm³ for Pb(II) whereas oxidation current depends linearly on cadmium concentration in the ranges 0.05–1.6 and 1.6–40μmol/dm³.

Calibration curves (Fig 12) were described by linear equations, correlation coefficients and limits of detection. The corresponding equations were for Pb(II)—I (μA) = (18.3±0.2) c
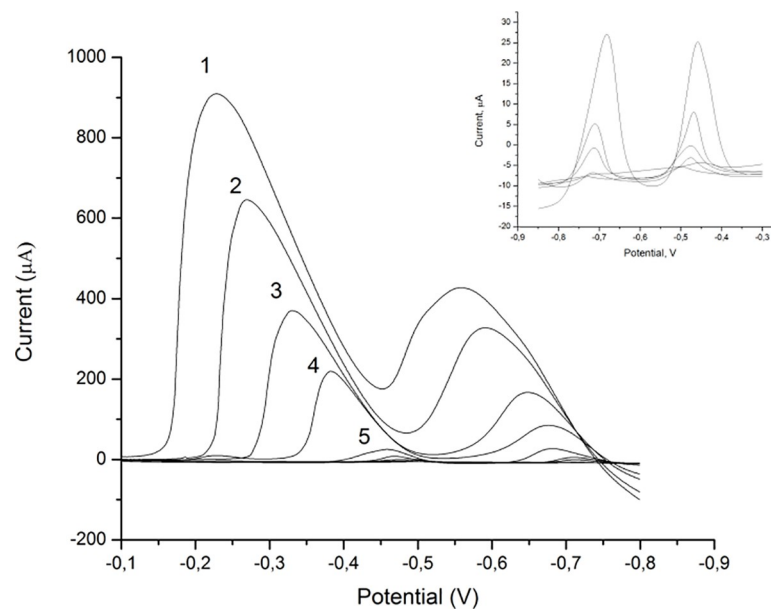

Fig 11. LSAS voltammograms obtained for Pb(II) and Cd(II) standard solutions for concentration range 1.6, 10, 20, 30 and 40 μmol/dm³, and the insert present voltammograms obtained for 0.05, 0.1, 0.2, 0.4, 0.8 and 1.6 μmol/dm³.
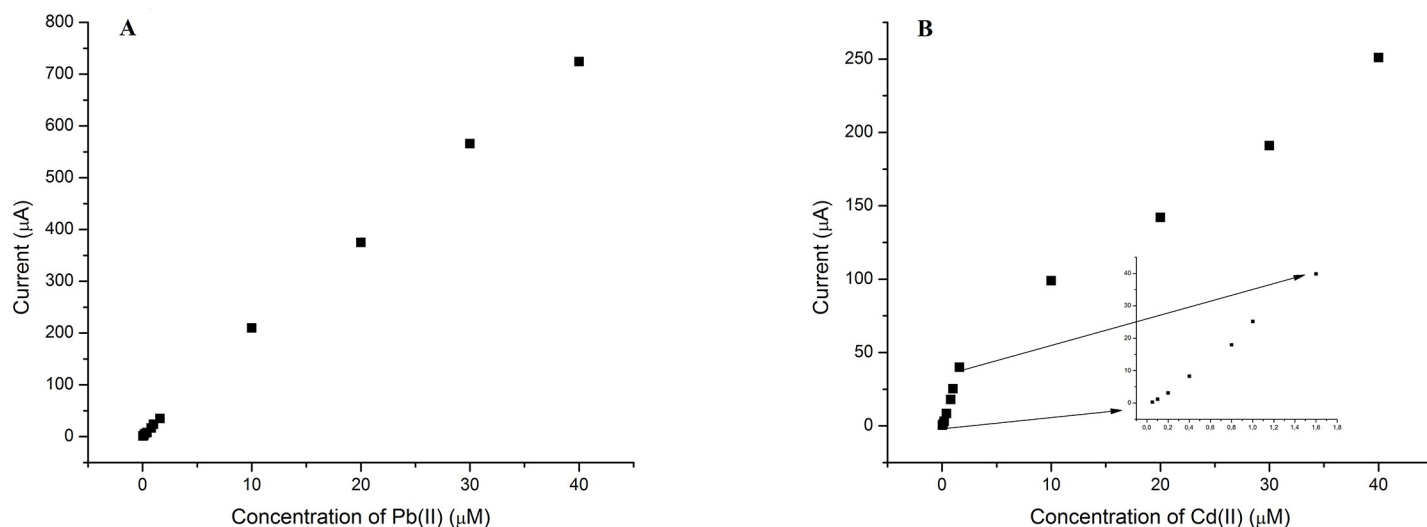
Fig 12. Calibration curves obtained for Pb(II) (A) and Cd(II) (B) in the concentration range 0.05–40 µmol/dm^3. Insert on B figure is calibration curve for Cd(II) in the range 0.05–1.6 µmol/dm^3.

(µmol/dm^3) + (5.2±0.3), correlation coefficient r^2 = 0.9987, and detection limit (calculated as 3S/b, where S is standard deviation of the intercept and b is the slope) was 1.67 ppb for Pb(II) and I (µA) = (25.9±0.5)c (µmol/dm^3)—(1.6±0.4), r^2 = 0.9973 and corresponding detection limit 0.79 ppb for lower Cd(II) concentration range and I (µA) = (5.3±0.2)c (µmol/dm^3) + (36.9±5.5), r^2 = 0.9929 for higher Cd(II) concentration range. One of the advantages of this sensor, beside sensitivity is its reproducibility. It was evaluated under optimal conditions for five repetitive measurements of 0.05 µmol/dm^3 for both Pb(II) and Cd(II) and corresponding relative standard deviations were 7.68% (Pb) and 3.46% (Cd). From presented results it can be concluded that this modification, MnCo$_2$O$_4$ particles, improves the sensitivity and the selectivity of the glassy carbon electrode. The sensor is easy to prepare, to use on cheap equipment and it analytical parameters are much better than some obtained by more sensitive electrochemical techniques (Table 2).

The new sensor was applied on determination of analytes in real samples. Standard addition of 0.5 µmol/dm^3 of both Pb(II) and Cd(II) caused increase of current at the sample potential and made the determination possible (Fig 13). The determination of lead and cadmium in three water samples are presented in Table 3. The results present average of three measurements, and the recovery is also calculated. The use of this sensor enabled determination of analytes in samples without complicated sample preparation. Also, these values are significantly lower than maximum allowed levels of lead and cadmium in drinking water given by the World Health Organization (10 µg/dm^3 for Pb and 3 µg/dm^3 for Cd) [60].

Conclusions

Porous MnCo$_2$O$_4$ spinel oxide was successfully synthesized by citrate-gel combustion technique. It was an interesting finding that this method of synthesis enabled simultaneous determination of two very toxic metals, lead and cadmium. The GCE-MnCo$_2$O$_4$NPs has shown excellent electrochemical properties such as fast current response, low detection limit and good selectivity due to unique structure. Under optimized conditions, the peak currents were increased with concentrations of metal ions linearly within two range 0.05–40 µmol/dm^3 of Pb (II) and 0.05–1.6 and 1.6–40 µmol/dm^3 of Cd(II). The detection limits for Pb(II) and Cd(II)

Table 2. Comparison of different modified electrodes for Pb(II) and Cd(II) determination.

Electrodes	Method	Pb(II)		Cd(II)		Ref.
		Linear range (μg/dm^3)	Detection limit (μg/dm^3)	Linear range (μg/dm^3)	Detection limit (μg/dm^3)	
Nafion-Bi/NMC/GCE	DPASV	0.5–100	0.05	2–200	1.5	[10]
MnO$_2$/GCE	LSASV	-	5.58	-	5.84	[33]
Cr$_2$O$_3$/CPE	SWASV	10–800	3	10–800	3	[11]
Cross-linkedchitosan/CNTPE	LSASV	NA	NA	6.6–168.6	1.1	[12]
AuNPs/CNFs	SWASV	20.72–207.2	20.72	11.24–112.4	11.2	[52]
SnO$_2$ quantumdots	CV	NA	NA	4990–44910	499	[61]
BiNPs/SPCE	SWASV	0–100	2	0–100	5	[50]
Bi-film/CE	SWASV	-	2.54	-	5.69	[62]
SNAC/GCE	DPASV	18.6–1181.0	1.2	10.1–539.6	2.7	[63]
COOH-C4	DPASV	280–2500	6.2	NA	-	[64]
MnCo$_2$O$_4$/GCE (coprecipitationmethodsynthesis)	DPSAV	NA	NA	2.3–120	0.72	[1]
GCE-MnCo$_2$O$_4$NPs (citrate-gelcombustionmethod	LSASV	10.4–8280	1.67	5.6–179.2	0.79	Thispaper

NMC/GCE: Nitrogendopedmicroporouscarbon/glassycarbonelectrode; CNTPE: Carbonnanotubepasteelectrode; AuNPs/CNFs: Aunanoparticles/carbonnanofibers; BiNPs/SPCE: Bismuthnanoparticles/screen-printedcarbonelectrode; CE:carbonelectrode; SNAC: sphericalcarbonnanoparticledecoratedactivatedcarbon; DPASV: differentialpulseanodicstrippingvoltammetry; SWASV: squarewaveanodicstrippingvoltammetry; NA: Notanalysed

were 1.67 and 0.79 μg/dm^3, respectively. Additional advantages of this method for determination of cadmium and lead are easily, green and inexpensive synthesis of porous MnCo$_2$O$_4$ spinel and very simple fabrication of modified GC electrode. The sensor was successfully validated on real water samples, therefore, it can be easily used as portable field device for onsite control of heavy metal concentration.
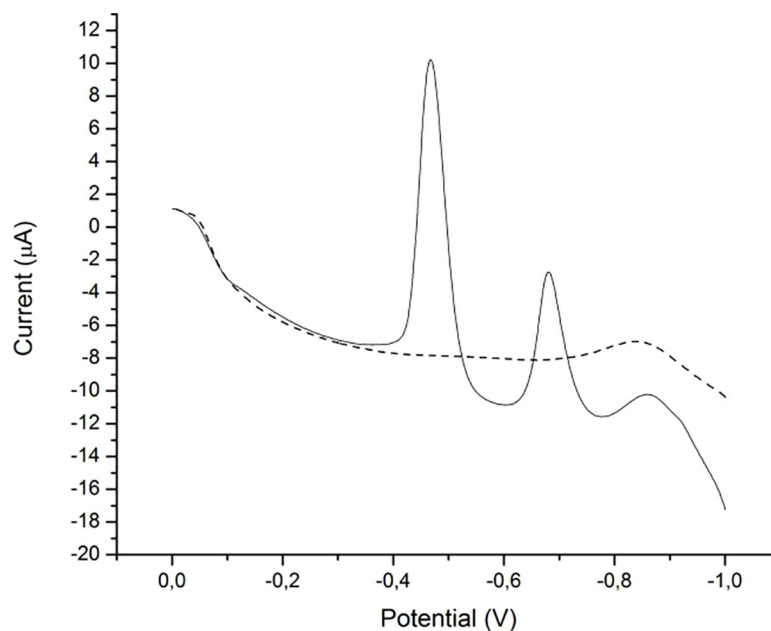

Fig 13. Voltammograms of river sample (dashed) and river sample spiked with 0.5 μmol/dm^{3}Pb(II) and Cd(II) (solid).

Table 3. Recovery tests for determination of Pb(II) and Cd(II) in water samples using GCE- MnCo$_2$O$_4$NPs (n.d.—not detectable; SD—standard deviation).

Sample	Analyte	Analyte in water before addition	Added (nmol/dm^3)	Found (nmol/dm^3)±SD	Recovery (%)
Distilled water	Pb(II)	n.d.	500.0	523.3±15.0	104.6
	Cd(II)	n.d.	500.0	504.2±22.1	100.8
Tap water	Pb(II)	n.d.	500.0	496.3±14.2	99.3
	Cd(II)	n.d.	500.0	487.5±21.4	97.5
River water	Pb(II)	n.d.	500.0	510.0±14.6	102
	Cd(II)	n.d.	500.0	548.0±24.1	109.6

https://doi.org/10.1371/journal.pone.0210904.t003

Author Contributions

Conceptualization: Vesna Antunović, Dijana Jelić, Aleksandar Lolić.

Investigation: Vesna Antunović.

Methodology: Rada Baošić, Dijana Jelić.

Resources: Marija Ilić.

Validation: Rada Baošić.

Writing – original draft: Vesna Antunović, Aleksandar Lolić.

References

1. Velmurugan M, Chen S-M. Synthesis and Characterization of Porous MnCo2O4 for Electrochemical Determination of Cadmium ions in Water Samples. Sci Rep [Internet]. 2017 Dec 5 [cited 2018 Jul 23]; 7 (1):653. Available from: http://www.ncbi.nlm.nih.gov/pubmed/28381862 https://doi.org/10.1038/s41598-017-00748-x PMID: 28381862

2. Naik KK, Khare RT, Gelamo R V, More MA, Thapa R, Late DJ, et al. Enhanced electron field emission from NiCo$_2$O$_4$ nanosheet arrays. Mater Res Express [Internet]. 2015 Sep 10 [cited 2018 Jul 23]; 2 (9):095011. Available from: http://stacks.iop.org/2053-1591/2/i=9/a=095011?key=crossref.4c09bbb7e49cd430349feff763427949

3. BARROS JM, BEZERRA MA, VALASQUES GS, NASCIMENTO BB DO JUNIOR, SOUZA AS, ARAGAO NM DE. Multivariate optimization of an ultrasound-assisted extraction procedure for Cu, Mn, Ni and Zn determination in ration to chickens. An Acad Bras Cienc [Internet]. 2013 Sep [cited 2018 Jul 23]; 85(3):891–902. Available from: http://www.ncbi.nlm.nih.gov/pubmed/24068081 https://doi.org/10.1590/S0001-37652013000300005 PMID: 24068081

4. Bagheri H, Afkhami A, Saber-Tehrani M, Khoshsafar H. Preparation and characterization of magnetic nanocomposite of Schiff base/silica/magnetite as a preconcentration phase for the trace determination of heavy metal ions in water, food and biological samples using atomic absorption spectrometry. Talanta [Internet]. 2012 Aug 15 [cited 2018 Jul 23]; 97:87–95. Available from: http://www.ncbi.nlm.nih.gov/pubmed/22841051 https://doi.org/10.1016/j.talanta.2012.03.066 PMID: 22841051

5. Batista BL, Rodrigues JL, de Oliveira Souza VC, Barbosa F. A fast ultrasound-assisted extraction procedure for trace elements determination in hair samples by ICP-MS for forensic analysis. Forensic Sci Int [Internet]. 2009 Nov 20 [cited 2018 Jul 23]; 192(1–3):88–93. Available from: http://www.ncbi.nlm.nih.gov/pubmed/19740615 https://doi.org/10.1016/j.forsciint.2009.08.003 PMID: 19740615

6. Wang H, Wu Z, Chen B, He M, Hu B. Chip-based array magnetic solid phase microextraction on-line coupled with inductively coupled plasma mass spectrometry for the determination of trace heavy metals in cells. Analyst [Internet]. 2015 Aug 21 [cited 2018 Jul 23]; 140(16):5619–26. Available from: http://www.ncbi.nlm.nih.gov/pubmed/26131454 https://doi.org/10.1039/c5an00736d PMID: 26131454

7. Hristozov D, Domini CE, Kmetov V, Stefanova V, Georgieva D, Canals A. Direct ultrasound-assisted extraction of heavy metals from sewage sludge samples for ICP-OES analysis. Anal Chim Acta [Internet]. 2004 Jul 19 [cited 2018 Jul 23]; 516(1–2):187–96. Available from: https://www.sciencedirect.com/science/article/pii/S0003267004004908

8. Losev VN, Buyko O V., Trofimchuk AK, Zuy ON. Silica sequentially modified with polyhexamethylene guanidine and Arsenazo I for preconcentration and ICP–OES determination of metals in natural waters. Microchem J [Internet]. 2015 Nov 1 [cited 2018 Jul 23]; 123:84–9. Available from: https://www.sciencedirect.com/science/article/pii/S0026265X15001198

9. Sitko R, Janik P, Zawisza B, Talik E, Margui E, Queralt I. Green Approach for Ultratrace Determination of Divalent Metal Ions and Arsenic Species Using Total-Reflection X-ray Fluorescence Spectrometry and Mercapto-Modified Graphene Oxide Nanosheets as a Novel Adsorbent. Anal Chem [Internet]. 2015 Mar 17 [cited 2018 Jul 23]; 87(6):3535–42. Available from: http://www.ncbi.nlm.nih.gov/pubmed/25707847 https://doi.org/10.1021/acs.analchem.5b00283 PMID: 25707847

10. Xiao L, Xu H, Zhou S, Song T, Wang H, Li S, et al. Simultaneous detection of Cd(II) and Pb(II) by differential pulse anodic stripping voltammetry at a nitrogen-doped microporous carbon/Nafion/bismuth-film electrode. Electrochim Acta [Internet]. 2014 Oct 10 [cited 2018 Jul 23]; 143:143–51. Available from: https://www.sciencedirect.com/science/article/pii/S0013468614016119

11. Koudelkova Z, Syrovy T, Ambrozova P, Moravec Z, Kubac L, Hynek D, et al. Determination of Zinc, Cadmium, Lead, Copper and Silver Using a Carbon Paste Electrode and a Screen Printed Electrode Modified with Chromium(III) Oxide. Sensors [Internet]. 2017 Aug 9 [cited 2018 Jul 23]; 17(8):1832. Available from: http://www.ncbi.nlm.nih.gov/pubmed/28792450

12. Janegitz BC, Figueiredo-Filho LCS, Marcolino-Junior LH, Souza SPN, Pereira-Filho ER, Fatibello-Filho O. Development of a carbon nanotubes paste electrode modified with crosslinked chitosan for cadmium (II) and mercury(II) determination. J Electroanal Chem [Internet]. 2011 Sep 1 [cited 2018 Jul 23]; 660 (1):209–16. Available from: https://www.sciencedirect.com/science/article/pii/S1572665711003377

13. Aktürk M, Karabiberoğlu ŞU, Dursun Z. Fabrication of Cu−CeO2 Coated Multiwall Carbon Nanotube Composite Electrode for Simultaneous Determination of Guanine and Adenine. Electroanalysis [Internet]. [cited 2018 Jul 23]; 30(2):238–49. Available from: https://onlinelibrary.wiley.com/doi/abs/10.1002/elan.201700590

14. Sun Y-F, Chen W-K, Li W-J, Jiang T-J, Liu J-H, Liu Z-G. Selective detection toward Cd2+ using Fe3O4/RGO nanoparticle modified glassy carbon electrode. J Electroanal Chem [Internet]. 2014 Feb 1 [cited 2018 Jul 23];714– 715:97–102. Available from: https://www.sciencedirect.com/science/article/pii/S1572665713005808

15. Mishra YK, Adelung R. ZnO tetrapod materials for functional applications. Mater Today [Internet]. 2018 Jul 1 [cited 2018 Dec 11]; 21(6):631–51. Available from: https://www.sciencedirect.com/science/article/pii/S1369702117304443

16. Sharma M, Joshi M, Nigam S, Shree S, Avasthi DK, Adelung R, et al. ZnO tetrapods and activated carbon based hybrid composite: Adsorbents for enhanced decontamination of hexavalent chromium from aqueous solution. Chem Eng J [Internet]. 2019 Feb 15 [cited 2018 Dec 11]; 358:540–51. Available from: https://www.sciencedirect.com/science/article/pii/S1385894718319727

17. Tripathi KM, Tran TS, Kim YJ, Kim T. Green Fluorescent Onion-Like Carbon Nanoparticles from Flaxseed Oil for Visible Light Induced Photocatalytic Applications and Label-Free Detection of Al(III) Ions. ACS Sustain Chem Eng [Internet]. 2017 May 6 [cited 2018 Dec 11]; 5(5):3982–92. Available from: http://pubs.acs.org/doi/10.1021/acssuschemeng.6b03182

18. Tripathi KM, Singh A, Bhati A, Sarkar S, Sonkar SK. Sustainable Feasibility of the Environmental Pollutant Soot to Few-Layer Photoluminescent Graphene Nanosheets for Multifunctional Applications. ACS Sustain Chem Eng [Internet]. 2016 Dec 5 [cited 2018 Dec 11]; 4(12):6399–408. Available from: http://pubs.acs.org/doi/10.1021/acssuschemeng.6b01045

19. Cheng F, Shen J, Peng B, Pan Y, Tao Z, Chen J. Rapid room-temperature synthesis of nanocrystalline spinels as oxygen reduction and evolution electrocatalysts. Nat Chem 2010 31 [Internet]. 2010 Dec 12 [cited 2018 Jul 23]; 3(1):79. Available from: https://www.nature.com/articles/nchem.931 https://doi.org/10.1038/nchem.931 PMID: 21160522

20. Imran M, Kim DH, Al-Masry WA, Mahmood A, Hassan A, Haider S, et al. Manganese-, cobalt-, and zinc-based mixed-oxide spinels as novel catalysts for the chemical recycling of poly(ethylene terephthalate) via glycolysis. Polym Degrad Stab [Internet]. 2013 Apr 1 [cited 2018 Jul 23]; 98(4):904–15. Available from: https://www.sciencedirect.com/science/article/pii/S0141391013000220

21. Zhou L, Zhao D, Lou XW. Double-Shelled CoMn$_2$O$_4$ Hollow Microcubes as High-Capacity Anodes for Lithium-Ion Batteries. Adv Mater [Internet]. 2012 Feb 7 [cited 2018 Jul 23]; 24(6):745–8. Available from: http://doi.wiley.com/10.1002/adma.201104407 PMID: 22213232

22. Gul IH, Ahmed W, Maqsood A. Electrical and magnetic characterization of nanocrystalline Ni–Zn ferrite synthesis by co-precipitation route. J Magn Magn Mater [Internet]. 2008 Feb 1 [cited 2018 Jul 23]; 320 (3–4):270–5. Available from: https://www.sciencedirect.com/science/article/abs/pii/S0304885307007470

23. Lavela P, Tirado JL, Vidal-Abarca C. Sol–gel preparation of cobalt manganese mixed oxides for their use as electrode materials in lithium cells. Electrochim Acta [Internet]. 2007 Nov 1 [cited 2018 Jul 23]; 52(28):7986–95. Available from: https://www.sciencedirect.com/science/article/pii/S0013468607008377

24. Zahi S, Hashim M, Daud AR. Synthesis, magnetic properties and microstructure of Ni–Zn ferrite by sol–gel technique. J Magn Magn Mater [Internet]. 2007 Jan 1 [cited 2018 Jul 23]; 308(2):177–82. Available from: https://www.sciencedirect.com/science/article/abs/pii/S0304885306008687

25. Košak A, Makovec D, Žnidaršič A, Drofenik M. Preparation of MnZn-ferrite with microemulsion technique. J Eur Ceram Soc [Internet]. 2004 Jan 1 [cited 2018 Jul 23]; 24(6):959–62. Available from: https://www.sciencedirect.com/science/article/pii/S0955221903005247

26. Liang Y, Wang H, Zhou J, Li Y, Wang J, Regier T, et al. Covalent Hybrid of Spinel Manganese–Cobalt Oxide and Graphene as Advanced Oxygen Reduction Electrocatalysts. J Am Chem Soc [Internet]. 2012 Feb 22 [cited 2018 Jul 23]; 134(7):3517–23. Available from: http://pubs.acs.org/doi/10.1021/ja210924t PMID: 22280461

27. Takayama A, Okuya M, Kaneko S. Spray pyrolysis deposition of NiZn ferrite thin films. Solid State Ionics [Internet]. 2004 Aug 31 [cited 2018 Jul 23]; 172(1–4):257–60. Available from: https://www.sciencedirect.com/science/article/abs/pii/S0167273804002528

28. Li C, Han X, Cheng F, Hu Y, Chen C, Chen J. Phase and composition controllable synthesis of cobalt manganese spinel nanoparticles towards efficient oxygen electrocatalysis. Nat Commun [Internet]. 2015 Dec 4 [cited 2018 Jul 23]; 6(1):7345. Available from: http://www.nature.com/articles/ncomms8345

29. Muneam H, Hadi S, Kareem MM, Jackson SD. Preparation and characterization of (Co,Mn)(Co,Mn)2O4/MgO catalysts. Int J Ind Chem [Internet]. 2016 Mar 22 [cited 2018 Jul 23]; 7(1):93–101. Available from: http://link.springer.com/10.1007/s40090-015-0069-1

30. Mondal A, Das S, Manam J. Hydrothermal synthesis, structural and luminescent properties of a Cr^{3+} doped $MgGa_2O_4$ near-infrared long lasting nanophospor. RSC Adv [Internet]. 2016 Aug 31 [cited 2018 Jul 23]; 6(86):82484–95. Available from: http://xlink.rsc.org/?DOI=C6RA15119A

31. Kale SB, Kalubarme RS, Mahadadalkar MA, Jadhav HS, Bhirud AP, Ambekar JD, et al. Hierarchical 3D $ZnIn_2S_4$/graphene nano-heterostructures: their in situ fabrication with dual functionality in solar hydrogen production and as anodes for lithium ion batteries. Phys Chem Chem Phys [Internet]. 2015 Nov 25 [cited 2018 Jul 23]; 17(47):31850–61. Available from: http://xlink.rsc.org/?DOI=C5CP05546F https://doi.org/10.1039/c5cp05546f PMID: 26568094

32. Zhang Y, Xuan H, Xu Y, Guo B, Li H, Kang L, et al. One-step large scale combustion synthesis mesoporous MnO2/MnCo2O4 composite as electrode material for high-performance supercapacitors. Electrochim Acta [Internet]. 2016 Jul 10 [cited 2018 Jul 23]; 206:278–90. Available from: https://www.sciencedirect.com/science/article/pii/S0013468616309847

33. Mališić M, Janošević A, Šljukić Paunković B, Stojković I, Ćirić-Marjanović G. Exploration of MnO2/carbon composites and their application to simultaneous electroanalytical determination of Pb(II) and Cd (II). Electrochim Acta [Internet]. 2012 Jul 15 [cited 2018 Jul 23]; 74:158–64. Available from: https://www.sciencedirect.com/science/article/pii/S0013468612006056

34. Maerle AA, Karakulina AA, Moskovskaya IF, Romanovskii B V. Mesoporous cobalt and manganese spinels: Synthesis and physicochemical properties. Russ J Phys Chem A [Internet]. 2017 May 21 [cited 2018 Jul 23]; 91(5):910–4. Available from: http://link.springer.com/10.1134/S003602441705017X

35. Pirogova GN, Panich NM, Korosteleva RI, Voronin Y V., Popova NN. Catalytic properties of chromites with a spinel structure in the oxidation of CO and hydrocarbons and reduction of nitrogen oxides. Russ Chem Bull [Internet]. 2001 [cited 2018 Jul 23]; 50(12):2377–80. Available from: http://link.springer.com/10.1023/A:1015083529355

36. Klissurski DG, Uzunova EL. Cation-deficient nano-dimensional particle size cobalt–manganese spinel mixed oxides. Appl Surf Sci [Internet]. 2003 May 31 [cited 2018 Jul 23]; 214(1–4):370–4. Available from: https://www.sciencedirect.com/science/article/pii/S0169433203005245

37. Stoilova D, Koleva V. IR study of solid phases formed in the Mg(HCOO)2–Cu(HCOO)2–H2O system. J Mol Struct [Internet]. 2000 Oct 10 [cited 2018 Jul 23]; 553(1–3):131–9. Available from: https://www.sciencedirect.com/science/article/abs/pii/S002228600000541X

38. Sutka A, Mezinskis G. Sol-gel auto-combustion synthesis of spinel-type ferrite nanomaterials. Front Mater Sci [Internet]. 2012 Jun 14 [cited 2018 Jul 23]; 6(2):128–41. Available from: http://link.springer.com/10.1007/s11706-012-0167-3

39. Chen D-H, He X-R. Synthesis of nickel ferrite nanoparticles by sol-gel method. Mater Res Bull [Internet]. 2001 May 1 [cited 2018 Jul 23]; 36(7–8):1369–77. Available from: https://www.sciencedirect.com/science/article/pii/S0025540801006201

40. Jelić D, Zeljković S, Škundrić B, Mentus S. Thermogravimetric study of the reduction of CuO–WO3 oxide mixtures in the entire range of molar ratios. J Therm Anal Calorim [Internet]. 2018 Apr 18 [cited 2018 Jul 23]; 132(1):77–90. Available from: http://link.springer.com/10.1007/s10973-017-6921-0

41. Modi KB, Chhantbar MC, Joshi HH. Study of elastic behaviour of magnesium ferri aluminates. Ceram Int [Internet]. 2006 Jan 1 [cited 2018 Jul 23]; 32(2):111–4. Available from: https://www.sciencedirect.com/science/article/pii/S027288420500043X

42. Bhujun B, Tan MTT, Shanmugam AS. Study of mixed ternary transition metal ferrites as potential electrodes for supercapacitor applications. Results Phys [Internet]. 2017 Jan 1 [cited 2018 Jul 23]; 7:345–53. Available from: https://www.sciencedirect.com/science/article/pii/S2211379716300134

43. Zhang Y, Liu S, Li Y, Deng D, Si X, Ding Y, et al. Electrospun graphene decorated MnCo2O4 composite nanofibers for glucose biosensing. Biosens Bioelectron [Internet]. 2015 Apr 15 [cited 2018 Dec 26]; 66:308–15. Available from: http://www.ncbi.nlm.nih.gov/pubmed/25437368 https://doi.org/10.1016/j.bios.2014.11.040 PMID: 25437368

44. Velmurugan M, Chen SM. Synthesis and characterization of porous MnCo2O4for electrochemical determination of cadmium ions in water samples. Sci Rep [Internet]. 2017; 7(1):1–8. Available from: http://dx.doi.org/10.1038/s41598-017-00748-x

45. Li T, Liao T, Su X, Yu X, Han B, Zhu Y, et al. Preparation of cobalt-containing spinel oxides as novel adsorbents for efficient phosphate removal. Environ Sci Water Res Technol [Internet]. 2018 Sep 27 [cited 2018 Dec 26]; 4(10):1671–84. Available from: http://xlink.rsc.org/?DOI=C8EW00517F

46. Jiang H, Zhao T, Li C, Ma J. Hierarchical self-assembly of ultrathin nickel hydroxide nanoflakes for high-performance supercapacitors. J Mater Chem [Internet]. 2011 Mar 1 [cited 2018 Dec 26]; 21(11):3818. Available from: http://xlink.rsc.org/?DOI=c0jm03830j

47. Wang K, Cai R, Yuan T, Yu X, Ran R, Shao Z. Process investigation, electrochemical characterization and optimization of LiFePO4/C composite from mechanical activation using sucrose as carbon source. Electrochim Acta [Internet]. 2009 Apr 12 [cited 2018 Sep 4]; 54(10):2861–8. Available from: http://linkinghub.elsevier.com/retrieve/pii/S0013468608013005

48. Chong J, Xun S, Song X, Ridgway P, Liu G, Battaglia VS. Towards the understanding of coatings on rate performance of LiFePO4. J Power Sources [Internet]. 2012 Feb [cited 2018 Sep 4]; 200:67–76. Available from: http://linkinghub.elsevier.com/retrieve/pii/S0378775311020660

49. Wanekaya AK. Applications of nanoscale carbon-based materials in heavy metal sensing and detection. Analyst [Internet]. 2011 Oct 10 [cited 2018 Dec 30]; 136(21):4383. Available from: http://xlink.rsc.org/?DOI=c1an15574a https://doi.org/10.1039/c1an15574a PMID: 21894336

50. Cadevall M, Ros J, Merkoçi A. Bismuth nanoparticles integration into heavy metal electrochemical stripping sensor. Electrophoresis [Internet]. 2015 Aug [cited 2018 Jul 23]; 36(16):1872–9. Available from: http://doi.wiley.com/10.1002/elps.201400609 PMID: 25994368

51. Dai H, Wang N, Wang D, Ma H, Lin M. An electrochemical sensor based on phytic acid functionalized polypyrrole/graphene oxide nanocomposites for simultaneous determination of Cd(II) and Pb(II). Chem Eng J [Internet]. 2016 Sep 1 [cited 2018 Jul 23]; 299:150–5. Available from: https://www.sciencedirect.com/science/article/pii/S1385894716305332

52. Zhang B, Chen J, Zhu H, Yang T, Zou M, Zhang M, et al. Facile and green fabrication of size-controlled AuNPs/CNFs hybrids for the highly sensitive simultaneous detection of heavy metal ions. Electrochim Acta [Internet]. 2016 Apr 1 [cited 2018 Jul 23]; 196:422–30. Available from: https://www.sciencedirect.com/science/article/pii/S0013468616304649

53. Hamdani M, Singh RN, Chartier P. Co 3 O 4 and Co-Based Spinel Oxides Bifunctional Oxygen Electrodes. Int J Electrochem Sci [Internet]. 2010 [cited 2018 Jul 23]; 5:556–77. Available from: www.electrochemsci.org

54. Munjal S, Khare N, Nehate C, Koul V. Water dispersible CoFe2O4 nanoparticles with improved colloidal stability for biomedical applications. J Magn Magn Mater [Internet]. 2016 Apr 15 [cited 2018 Jul 23]; 404:166–9. Available from: https://www.sciencedirect.com/science/article/abs/pii/S0304885315308775

55. Gumpu MB, Veerapandian M, Krishnan UM, Rayappan JBB. Simultaneous electrochemical detection of Cd(II), Pb(II), As(III) and Hg(II) ions using ruthenium(II)-textured graphene oxide nanocomposite. Talanta [Internet]. 2017 Jan 1 [cited 2018 Jul 23]; 162:574–82. Available from: https://www.sciencedirect.com/science/article/pii/S003991401630830X https://doi.org/10.1016/j.talanta.2016.10.076 PMID: 27837874

56. Anandhakumar S, Mathiyarasu J, Narasimha Phani KL. Anodic stripping voltammetric determination of cadmium using a "mercury free" indium film electrode. Analyst [Internet]. 2013 Aug 28 [cited 2018 Jul 23]; 138(19):5674. Available from: http://xlink.rsc.org/?DOI=c3an01070h https://doi.org/10.1039/c3an01070h PMID: 23907152

57. Stanković DM, Škrivanj S, Savić N, Nikolić AS, Vulić P, Manojlović DD. Application of Novel Zn-Ferrite Modified Glassy Carbon Paste Electrode as a Sensor for Determination of Cd(II) in Waste Water. Electroanalysis [Internet]. 2014 Jul [cited 2018 Jul 23]; 26(7):1536–43. Available from: http://doi.wiley.com/10.1002/elan.201400095

58. Newman JS, Thomas-Alyea KE. Electrochemical systems [Internet]. J. Wiley; 2004 [cited 2018 Jul 23]. 647 p. Available from: https://www.wiley.com/en-us/Electrochemical+Systems%2C+3rd+Edition-p-9780471477563

59. Crowley K, Cassidy J. Trace Analysis of Lead at a Nafion-Modified Electrode Using Square-Wave Anodic Stripping Voltammetry. Electroanalysis [Internet]. 2002 Aug [cited 2018 Jul 23]; 14(15–16):1077–82. Available from: http://doi.wiley.com/10.1002/1521-4109%28200208%2914%3A15/16%3C1077%3A%3AAID-ELAN1077%3E3.0.CO%3B2-3

60. World Health Organization. Guidelines for drinking-water quality. World Health Organization; 2011. 541 p.

61. Bhanjana G, Dilbaghi N, Kumar R, Umar A, Kumar S. Sno2 quantum dots as novel platform for electrochemical sensing of cadmium. Electrochim Acta [Internet]. 2015 Jul 1 [cited 2018 Jul 23]; 169:97–102. Available from: https://www.sciencedirect.com/science/article/pii/S0013468615009238

62. Lee G-J, Kim CK, Lee MK, Rhee CK. Simultaneous Voltammetric Determination of Zn, Cd and Pb at Bismuth Nanopowder Electrodes with Various Particle Size Distributions. Electroanalysis [Internet]. 2010 Mar [cited 2018 Jul 23]; 22(5):530–5. Available from: http://doi.wiley.com/10.1002/elan.200900356

63. Madhu R, Sankar KV, Chen S-M, Selvan RK. Eco-friendly synthesis of activated carbon from dead mango leaves for the ultrahigh sensitive detection of toxic heavy metal ions and energy storage applications. RSC Adv [Internet]. 2014 Nov 28 [cited 2018 Jul 23]; 4(3):1225–33. Available from: http://xlink.rsc.org/?DOI=C3RA45089A

64. Nur Abdul Aziz SF, Zawawi R, Alang Ahmad SA. An Electrochemical Sensing Platform for the Detection of Lead Ions Based on Dicarboxyl-Calix[4]arene. Electroanalysis [Internet]. 2018 Mar [cited 2018 Jul 23]; 30(3):533–42. Available from: http://doi.wiley.com/10.1002/elan.201700736